

RESEARCH ARTICLE

10.1002/2017JC012911

Dense shelf water spreading from Antarctic coastal polynyas to the deep Southern Ocean: A regional circumpolar model study

Kazuya Kushara¹ , Guy D. Williams^{1,2} , Takeshi Tamura^{1,3,4} , Robert Massom^{1,5}, and Hiroyasu Hasumi⁶ 

Key Points:

- Passive tracer experiments detail the export of DSW formed in Antarctic coastal polynyas to the offshore basins of the Southern Ocean
- Nine key pathways of DSW over the Southern Ocean are described
- The contributions of regional DSW formation and distributions are estimated

Supporting Information:

- Supporting Information S1
- Movie S1

Correspondence to:

K. Kushara,
kazuya.kusahara@gmail.com

Citation:

Kusahara, K., G. D. Williams, T. Tamura, R. Massom, and H. Hasumi (2017), Dense shelf water spreading from Antarctic coastal polynyas to the deep Southern Ocean: A regional circumpolar model study, *J. Geophys. Res. Oceans*, 122, 6238–6253, doi:10.1002/2017JC012911.

Received 24 MAR 2017

Accepted 6 JUL 2017

Accepted article online 8 JUL 2017

Published online 4 AUG 2017

¹Antarctic Climate & Ecosystems Cooperative Research Centre, University of Tasmania, Hobart, Tasmania, Australia, ²Institute of Marine and Antarctic Studies, University of Tasmania, Hobart, Tasmania, Australia, ³National Institute of Polar Research, Tachikawa, Tokyo, Japan, ⁴SOKENDAI (The Graduate University of Advanced Studies), Tachikawa, Tokyo, Japan, ⁵Australia Antarctic Division, Kingston, Tasmania, Australia, ⁶Atmosphere and Ocean Research Institute, The University of Tokyo, Kashiwa, Chiba, Japan

Abstract The spreading of dense shelf water (DSW) from Antarctic coastal margins to lower latitudes plays a vital role in the ocean thermohaline circulation and the global climate system. Through enhanced localized sea ice production in Antarctic coastal polynyas, cold and saline DSW is formed over the continental shelf regions as a precursor to Antarctic Bottom Water (AABW). However, the detailed fate of coastal DSW over the Southern Ocean is still unclear. Here we conduct extensive passive tracer experiments using a circumpolar ocean-sea ice-ice shelf model to investigate pathways of the regional polynya-based DSW from the Antarctic margins to the deep Southern Ocean basins. In the numerical experiments, the Antarctic coastal margin is divided into nine regions, and a passive tracer is released from each region at the same rate as the local sea ice production. The modeled spatial distribution of the total concentration of the nine tracers is consistent with the observed AABW distribution and clearly demonstrates nine routes of the DSW over the Southern Ocean along its bottom topography. Furthermore, the model shows that while ~50% of the total tracer is distributed northward from the continental shelf to the deep ocean, ~7% is transported poleward beneath ice shelf cavities. The comprehensive tracer experiments allow us to estimate the contribution of local DSW to the total concentration along each of the pathways.

1. Introduction

Dense water formation in the polar regions is a key process for global ocean meridional overturning circulation with timescales of more than 1000 years [Schmitz, 1995]. Antarctic Bottom Water (AABW) is the densest water mass in global scale and occupies the largest volume on the ocean floor [Johnson, 2008]. The spreading of dense water to lower latitudes from Antarctic coastal margins plays a major role in regulating the denser and southern part of the meridional overturning circulation [Schmitz, 1995]. Along with this pumping of the “ocean conveyor belt,” a vast amount of nutrients and atmospheric gases are transported from the ocean surface to the abyssal layer, playing a pivotal role in the biogeochemical cycling of the Southern Ocean [Sigman and Boyle, 2000].

In the Southern Hemisphere, dense water is fundamentally formed around the Antarctic coastal margin as a result of enhanced sea ice formation in latent heat polynyas (also known as “coastal polynyas”) [Massom *et al.*, 1998; Morales Maqueda *et al.*, 2004]. Here massive ocean heat losses due to the direct contact between the relatively warm ocean surface and the very cold air from the Antarctic continent and ice sheet leads to high rates of sea ice production in freezing seasons [Tamura *et al.*, 2008]. The associated brine rejection (salinity input to the ocean from the process of sea ice formation) can substantially increase the density of coastal waters over the continental shelf regions. Thus, coastal polynyas can generate cold, saline dense shelf water (DSW) capable of producing AABW [Morales Maqueda *et al.*, 2004]. Once DSW is exported across the shelf break, its negative buoyancy relative to the offshore water masses causes it to sink down the continental slope [Baines and Condie, 1998]. On the slope, dense water increases in volume and is modified in its properties through entrainment of less dense ambient water masses, i.e., Antarctic Surface Water (AASW) and Circumpolar Deep Water (CDW).

Several studies based on oceanographic observations indicate decadal trends (particularly freshening signals) in deep and bottom water properties over the Southern Ocean that remain unexplained [e.g., Aoki *et al.*, 2005; Rintoul, 2007; Purkey and Johnson, 2013]. The changes in the deep ocean are not uniform in

space, indicating regional changes in DSW formation processes over the continental shelf regions. Improved knowledge about the detailed pathways of DSW on the decadal timescale is required for better understanding these recent changes in the Southern Ocean bottom water properties.

There have been several modeling studies on the pathways of AABW across the Southern Ocean. *Doney and Hecht* [2002] and *Santoso and England* [2008] investigated modeled AABW pathways, using passive tracers in coarse resolution models. Their horizontal resolutions ($>3.6^\circ$) were suitable for long-term integration, but too coarse to realistically resolve the bottom topography of the Southern Ocean and to reproduce Antarctic coastal processes for dense water formation. *Sasai et al.* [2004] showed that a global eddy-resolving ocean model (0.1°) could realistically reproduce the observed distribution of chlorofluorocarbon compounds (CFCs) [*Orsi et al.*, 1999]. However, their model did not have a sea ice component and mimicked the Antarctic coastal processes by restoring observed temperature and salinity near the southern coastal boundary. In a different approach, *Van Sebille et al.* [2013] used Lagrangian parcels, which were constantly released near the surface south of 60°S , and traced the parcels to identify the circulation of the deep and bottom waters. These studies clearly demonstrated that numerical modeling is a useful tool for better understanding the behavior of dense waters over the Southern Ocean. However, until now, there has been no modeling study which resolves the key coastal processes along Antarctic margins, i.e., high sea ice production and DSW formation in coastal polynyas, the interplay with ocean-ice shelf interactions and the connection of dense water from the continental shelf to the deep ocean. Moreover, there has been no work on regional dense water pathways.

Here in order to investigate detailed pathways of the dense water over the Southern Ocean, we use a high-resolution ocean-sea ice-ice shelf model to represent associated Antarctic coastal processes and bottom topography. In particular, we focus on DSW spreading from Antarctic coastal margins to the deep Southern Ocean on the decadal timescale. Using this model, we conduct extensive passive tracer experiments to identify not only the distribution of coastal DSW in deep Southern Ocean basins but also the regional contribution to the total bottom tracer distribution.

2. Numerical Model and Passive Tracer Experiments

This study used a coupled ocean-sea ice-ice shelf model described in *Kusahara and Hasumi* [2013, 2014]. The model domain was the circumpolar Southern Ocean. The northern boundary was placed at around 35°S as a solid wall. The horizontal resolution was 10–20 km over Antarctic coastal regions, allowing the representation of coastal protrusions, which provide an important “blocking effect” on sea-ice advection from upstream that promotes the formation of Antarctic coastal polynyas (persistent areas of open-ocean or thin-ice downwind/downstream of the boundaries). Subsequently, the model can reproduce high sea ice growth rates in key polynya regions and the associated dense water formation over the continental shelves [*Marsland et al.*, 2004, 2007; *Kusahara et al.*, 2010, 2011]. We used the RTopo-1 data set [*Timmermann et al.*, 2010] to specify bathymetry and ice shelf draft in the model. The model has 89 vertical levels: 4 grids for the surface σ layers, 49 grids with 40 m thickness between 40 and 2000 m, and 36 grids with 100 m thickness below 2000 m. Within six grids of the artificial northern boundary, ocean properties (e.g., temperature and salinity) were restored to the monthly mean climatology [*Steele et al.*, 2001] throughout the water column with a 10 day damping timescale. Sea surface salinity in the offshore region (>120 km from the Antarctic coastline) was restored to the monthly climatology to suppress deep convection in some regions (the Weddell and Ross Seas). A surface mixed layer parameterization based on turbulent closure [*Noh and Kim*, 1999] was used except where turned off under the ice shelves. Unstable stratification was removed by a simple convective adjustment scheme. We calculated surface boundary conditions from a climatological atmospheric surface data set (which has daily variability and a correction for katabatic winds) [*Röske*, 2006], and performed a 40 year simulation. With this configuration, sea ice production and modeled ice shelf basal melting reached a quasi steady state after a 15 year integration [*Kusahara et al.*, 2015].

We performed online passive tracer experiments, in which each coastal tracer was released at the same rate as the local sea ice production (SIP, seawater equivalent) and was passively transported by ocean currents in the model. The tracer was released only when sea ice formed. The tracer concentration represents the fraction of the source water, which comes from coastal sea ice formation. We diagnosed the salinity associated with brine rejection, by multiplying the tracer concentration and a factor $(S_{\text{ref}} - S_i)$, where S_{ref} and S_i

were reference salinities of the ocean (34.5 psu) and sea ice (5 psu), respectively. This method allows us to clearly trace high salinity water released from the coastal sea ice formation process, and thus we used the unit of salinity for the passive tracer.

We categorized the Antarctic coastal region into nine groups based on location (labels a–i in Figure 1a) and independently released the passive tracers to investigate the behavior of the regional dense shelf waters. With this grouping, we could discriminate the high sea ice areas and identify the origin of dense waters located offshore on the ocean floor. We performed a 25 year integration (16–40th model year) for the tracer experiments. The initial condition for the passive tracers was set to zero over the entire model domain. Outside the tracer source regions, the passive tracers were removed at the surface six grids (i.e., 120 m layer) and throughout the water column at the northern artificial boundary to avoid contamination of the surface and border effects.

3. Modeled Sea Ice Production, Mixed Layer Depth, and Overturning Circulation

3.1. Sea Ice Production Along Antarctic Coastal Margins

Sea ice production is the surface boundary condition for the passive tracers. A map of the modeled annual sea ice production averaged over the final 10 years (31–40th model year) is shown in Figure 1b. The modeled and observed sea ice edges in winter (an average over July–September) are superimposed on Figure 1 to show the model's representation of sea ice. Although there are some regional biases in the winter sea extent, the model reproduces the observed seasonal cycle of Antarctic sea ice in a reasonable fashion [Kusahara *et al.*, 2015]. Looking at the map of sea ice production, several active sea ice formation regions are identified along the Antarctic coastal margins. These high production areas correspond to winter coastal polynyas, which are located in coastal shelf regions shallower than 1000 m. The Ross Sea has an extensive area of very active sea ice production (>20 m/yr) in front of the Ross Ice Shelf. In the East Antarctic region, several small but productive coastal polynyas on the western side of topographic features are realistically reproduced, including important coastal polynyas at Cape Darnley, Mackenzie Bay, Barrier Bay, Shackleton Ice Shelf, Vincennes Bay, and Mertz Glacier. The broad Weddell Sea Polynya region has intermediate sea ice production of about 10 m/yr. The Eastern Weddell Sea and Amundsen-Bellinghshausen seas are characterized by relative low sea ice production. Overall, the modeled distribution of sea ice production is consistent with satellite-based observations [Tamura *et al.*, 2008; Nihashi and Ohshima, 2015], although there are some differences between the two. For example, the modeled sea ice production area in the Weddell Sea is wider than that observed. The difference may be due to an absence of fast ice-polynya interaction in the model [Nihashi and Ohshima, 2015] and/or underestimation of the observed sea ice production in thick ice regions [Tamura *et al.*, 2008; Kusahara *et al.*, 2010].

3.2. Annual Maximum Mixed Layer Depth

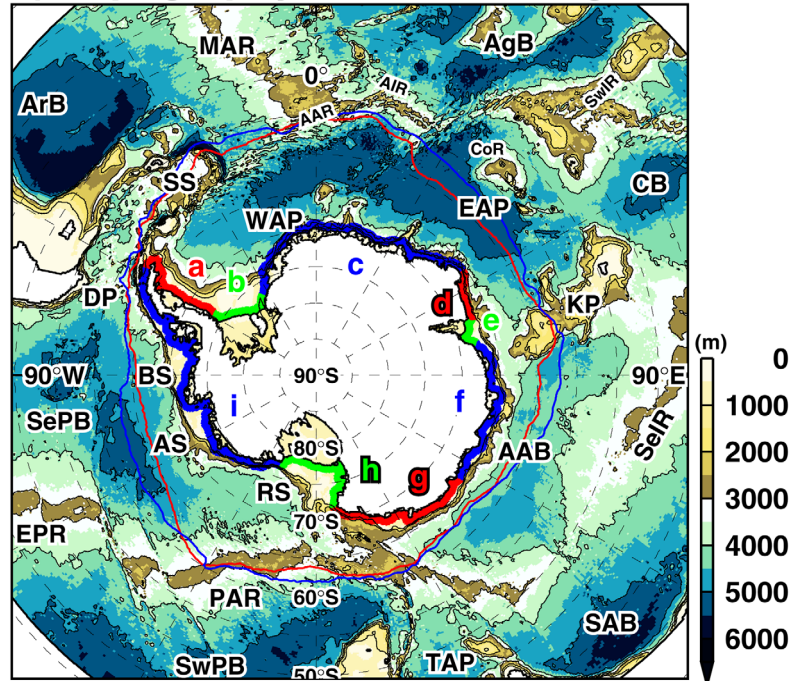
Consistent with the locations of high sea ice production in the coastal polynyas, areas of deep convection are produced over the Antarctic continental shelf regions (Figure 2a). We used a potential density threshold of 0.01 kg m^{-3} to define the surface mixed layer depth. Denser surfaces outcrop in several continental shelf regions (particularly in the Weddell and Ross Seas and the region $140\text{--}150^\circ\text{E}$) and the surface mixed layer is deep enough to reach the bottom (Figure 2b). These results clearly show that Antarctic coastal polynyas play an important role in connecting the ocean surface to deep and bottom layers.

Except for Antarctic coastal regions, the mixed layer depth in the seasonal sea ice zone is shallow (~ 100 m). North of 55°S , a relatively deep mixed layer is present in the Indian and Pacific Ocean sectors. The modeled pattern of the surface mixed layer depth over the Southern Ocean is consistent with that estimated from observational data sets [de Boyer Montégut *et al.*, 2004; Violaine *et al.*, 2017].

3.3. Overturning Circulation in the Southern Ocean

Salt input from active sea ice formation along Antarctic coastal margins is one of the essential processes in forming the lower limb of the deep meridional overturning circulation over the Southern Ocean (Figure 3). The modeled deep meridional circulation is reproduced in potential density larger than 27.82 kg m^{-3} , with a magnitude of approximately 18 Sv. It should be noted that while there is a wide range of estimates in the literature for the deep meridional circulation in the Southern Ocean (i.e., circumpolar AABW production rates from near-zero to 28 Sv), recent estimates tend to converge near 20 Sv [Jacobs, 2004]. The modeled

a) Topography and Source regions



b) Sea ice production

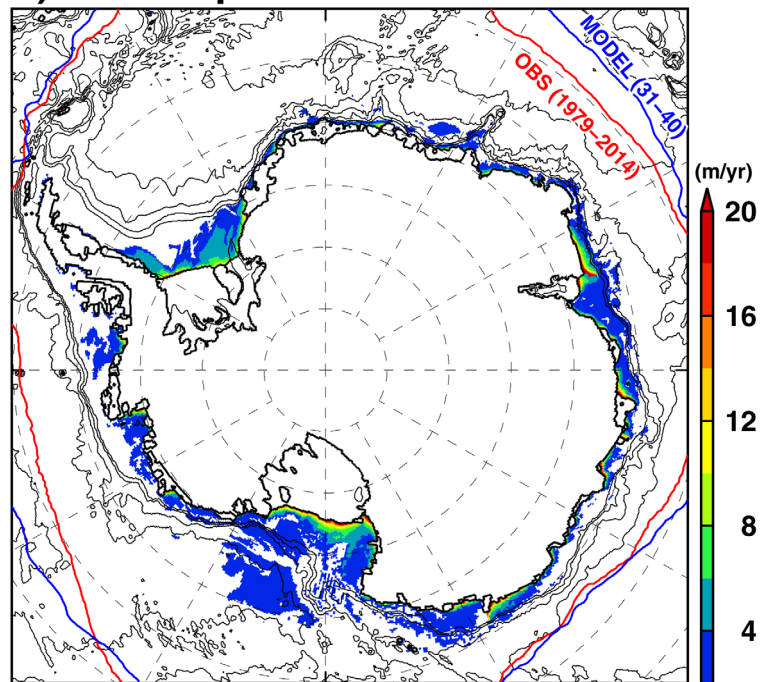
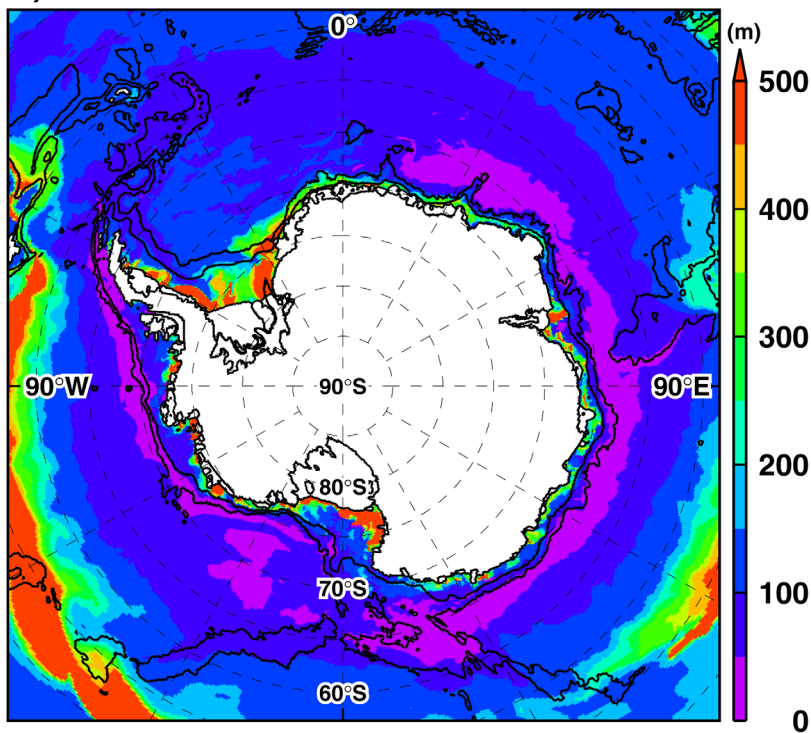


Figure 1. (a) Model bottom topography and (b) modeled annual sea ice production. In Figure 1a, nine coastal regions (labels a–i) are shown by different colors (red, green, or blue), and the observed and modeled wintertime (July–September average) sea ice edges are shown as color lines (red: satellite observation for 1979–2014, blue: the modeled average for the last 10 years). In Figure 1b, areas of sea ice production less than 2 m/yr are masked out. Place names used in the text are shown in Figure 1a: Argentine Basin (ArB), Scotia Sea (SS), Weddell Abyssal Plain (WAP), Mid-Atlantic Ridge (MAR), America–Antarctica Ridge (AAR), Atlantic–Indian Ridge (AIR), Agulhas Basin (AgB), Southwest Indian Ridge (SwIR), Conrad Rise (CoR), Crozet Basin (CB), Enderby Abyssal Plain (EAP), Kerguelen Plateau (KP), Southeast Indian Ridge (SeIR), Australian–Antarctic Basin (AAB), South Australian Basin (SAB), Tasman Abyssal Plain (TAP), Southwestern Pacific Basin (SwPB), Pacific–Antarctic Ridge (PAR), Ross Sea (RS), East Pacific Rise (EPR), Southeastern Pacific Basin (SePB), Amundsen Sea (AS), Bellingshausen Sea, (BS) and Drake Passage (DP). The black lines show depth contours, with a 1000 m interval.

a) Annual Maximum MLD



b) Annual Maximum MLD / Depth

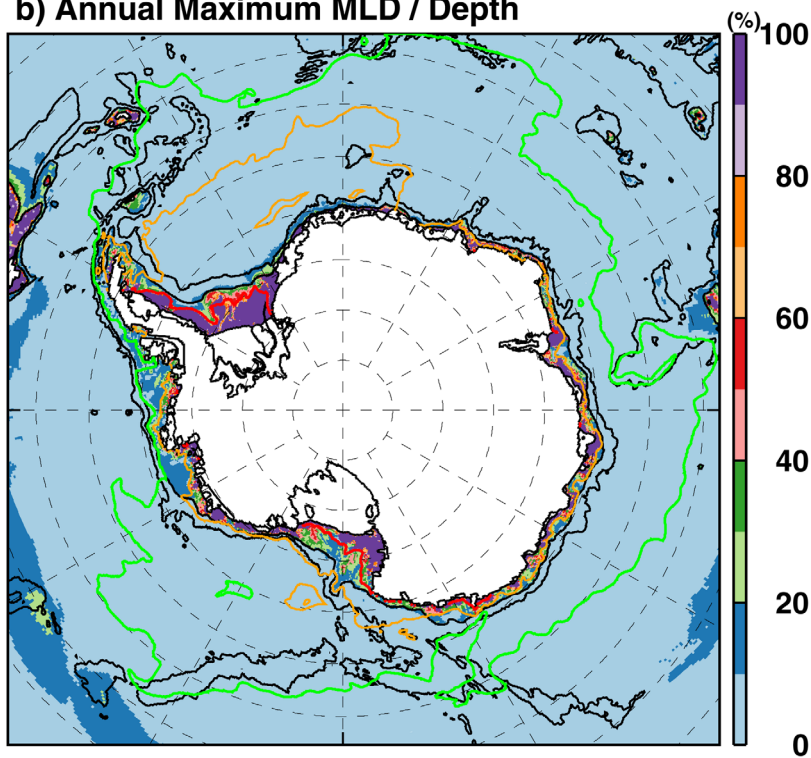


Figure 2. Maps of (a) annual maximum mixed layer depth and (b) the percentage of the mixed layer depth to local water depth. In Figure 2b, potential density surfaces of 27.8, 27.5, and 27.2 kg m⁻³ are shown by red, yellow, and green contours, respectively. The back lines show 1000 and 3000 m depth contours.

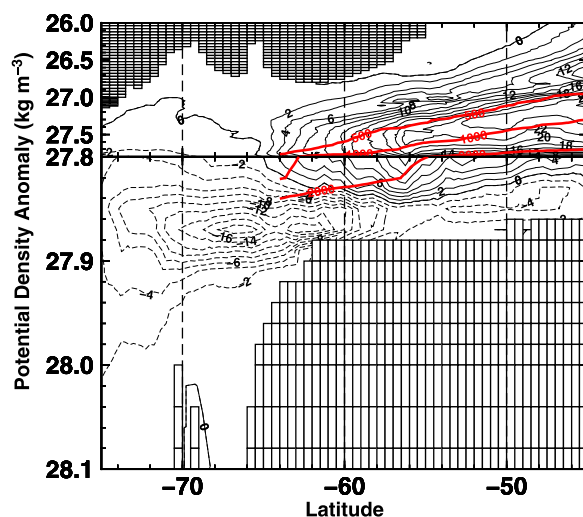


Figure 3. Stream function of zonally integrated meridional overturning circulation in the latitude-density space for the period from the 31st to the 40th model year. The vertical axis is potential density anomaly referenced to the surface, and the scales are different above and below the potential density of 27.80 kg m^{-3} . Negative values of the stream function (shown by dashed contours) indicate anticlockwise circulation. Red contours with labels indicate the zonal-average depth of the potential density.

in the depth-latitude domain are shown in Figure 5. The percentage of the total tracer distribution based on the location and density/depth is summarized in Table 1. Since the surface inputs of the passive tracers occurred repeatedly every year, the amount of the total tracer in the model domain increases almost linearly with the model integration. Thus, it is difficult for a regional Southern Ocean model to obtain a steady state for the passive tracer fields. However, after a 15 year integration, the distribution of the total tracer tends to converge in terms of regional and vertical tracer ratios to the total amount of the total tracer in the model domain (Figure 6), enabling us to examine the distributions of the tracers in detail at the end of the integration. Horizontal distribution of the total tracer at the ocean floor (the bottom-most cell) at the end of the integration is shown in Figure 7. A movie of the total tracer for the 25 year integration is available in supporting information, and clearly shows the time evolution of the total tracer distribution at the ocean floor.

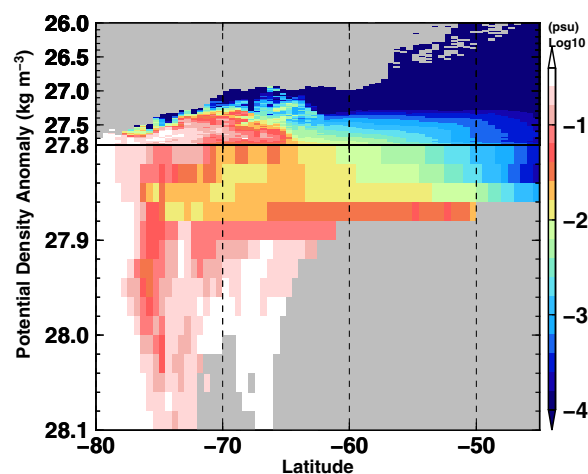


Figure 4. Vertical distribution of the zonal mean of the total tracer at the end of a 25 year integration (40th model year) in the latitude-density domain. Scales of the vertical axis are different above and below the potential density of 27.80 kg m^{-3} .

northward volume transport of the deep cell across 60°S is approximately 10 Sv, consistent with an observational AABW transport across the continental rise of 8.1 Sv [Orsi *et al.*, 2002]. Coastal passive tracers are advected from the Antarctic coastal surface to the deep Southern Ocean at lower latitudes within this deep meridional circulation.

4. Passive Tracer Distributions

4.1. Total Tracer (Sum of the Nine Regional Tracers)

Here we show vertical and horizontal distributions of a total tracer at the end of a 25 year integration of the passive tracers experiments to examine pathways of DSW originating from coastal polynyas. The total tracer is a sum of the nine regional passive tracers. Zonal mean distribution of the total tracer in the density-latitude domain is shown in Figure 4. Along selected longitudes (0° , 90°E , 180° , and 90°W), vertical tracer distributions

While here we use the tracer distribution at the ocean floor to describe the DSW pathways, distributions of the tracer integrated in the layer denser than 27.80 kg m^{-3} are shown in Appendix A. These two distributions are generally similar but the integrated tracer distribution is more extensive than the tracer at the ocean floor, reflecting rapid transport at intermediate depths by the Antarctic Circumpolar Current.

Looking at Figures 4–6 and Table 1, more than 70% of the total tracer is present in the higher density classes ($\sigma_\theta > 27.80 \text{ kg m}^{-3}$). A northward extension of the high concentration ($>10^{-2}$, yellow to red) is found in the potential density range of $27.84\text{--}27.86 \text{ kg m}^{-3}$ (Figure 4), and the signal is also confirmed in the bottom layers along the 90°E and 180° sections (Figures 5b and 5c). At the

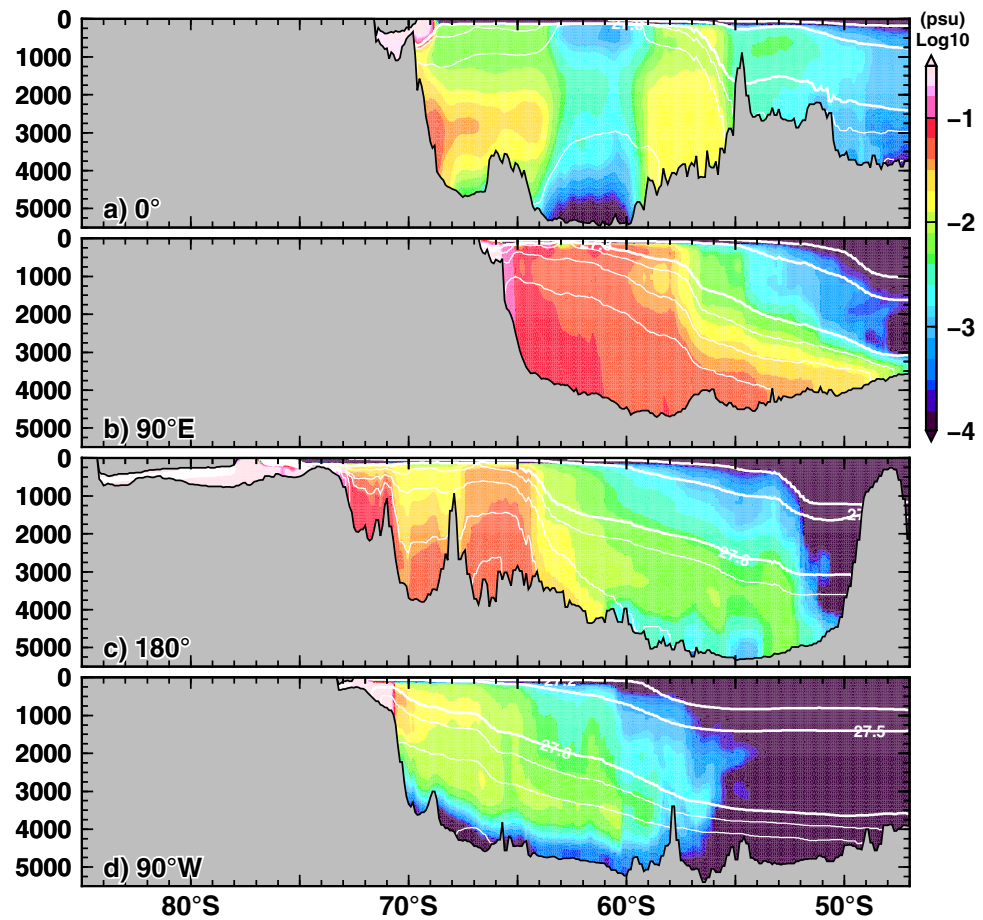


Figure 5. Vertical distribution of the total tracer at the end of a 25 year integration (40th model year) in the depth-latitude domain along four sections (a: 0°, b: 90°E, c: 180°, and d: 90°W). White contours show the potential density anomaly (thick lines for 27.20, 27.50, and 27.80 kg m⁻³, and thin lines with a 0.02 kg m⁻³ interval in the layers denser than 27.80 kg m⁻³).

initial stage of the tracer experiments, more than half of the total tracer remains in the source regions and ice shelf cavities (Figure 6). After the 15 year integration, the portion of the tracer near source regions becomes less than 20%, likely approaching an asymptotic state in the regional Southern Ocean system.

Looking at Figure 7, extensive zones of high passive tracer concentrations (>10⁻², yellow to red) occur not only in coastal regions but also in the deep ocean basins (see also supporting information Movie S1). A large part of the total tracer (>70%) is directly transported to the continental slope/rise and basin regions (see the line of the total tracer in Table 1), with the pathways being controlled by the bottom topography. The tracer concentration is high over the continental shelf regions and becomes lower on the deep ocean floor,

Table 1. Distribution (%) of the Passive Tracers: Total and Regional Tracers at the End of a 25 Year Integration of the Tracer Experiments

	Source Region	Ice Shelf	$\sigma_0 < 27.8 \text{ kg m}^{-3}$	$\sigma_0 \geq 27.8 \text{ kg m}^{-3}$ d < 2000 m	$\sigma_0 \geq 27.8 \text{ kg m}^{-3}$ d \geq 2000 m
Total (sum of the nine tracers)	14.3	6.6	8.2	25.4	45.5
Tracer a (Antarctic Peninsula)	9.8	2.9	13.1	31.6	42.6
Tracer b (Filchner-Ronne Ice Shelf)	8.0	12.1	6.2	27.3	46.4
Tracer c (Eastern Weddell Sea)	22.1	16.0	14.3	19.3	28.3
Tracer d (Cape Darnley)	6.7	0.1	11.2	27.2	54.8
Tracer e (Prydz Bay)	11.8	7.4	11.7	24.3	44.8
Tracer f (80–130°E)	14.4	3.2	14.7	28.9	38.8
Tracer g (Wilkes Land)	7.2	0.5	5.0	27.3	60.0
Tracer h (Ross Sea)	10.4	9.2	1.7	23.4	55.3
Tracer i (Amundsen-Bellingshausen seas)	33.8	9.8	7.3	23.8	25.3

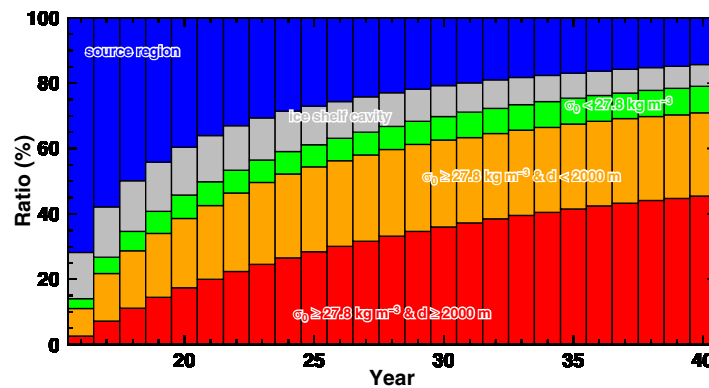


Figure 6. Time evolution of the ratio of the location and density/depth of the total tracer. See Figure 1a for the source regions and ice shelf cavities.

indicating active mixing between the dense shelf water with less dense ambient waters over the continental slope/rise and basin regions. High concentration regions of the total tracer ($>10^{-1}$, pink) are also found under the ice shelf cavities ($\sim 7\%$ of the total tracer), confirming that the newly formed DSW contributes to melting processes at the ice shelf base [Jacobs *et al.*, 1992; Kushara and Hasumi, 2013]. There is a sharp contrast in the total concentration on the continental shelf in the Amundsen-Bellinghousen seas. As shown in Figure 1b, sea ice formation is less in the Amundsen-Bellinghousen seas, and thus there is no active local DSW export to the deep ocean there.

The model clearly demonstrates nine main routes of the total tracer over the Southern Ocean, as shown in Figure 7. There are: (A1) a northward extension along the western flank of the Argentine Basin; (A2) a pathway from the Scotia Sea to the Argentine Basin in the Weddell Abyssal Plain; (A3) an eastward extension along the southern flank of the America-Antarctica Ridge; (E1) a northward extension between the southwestern Indian Ridge and the Kerguelen Plateau in the Enderby Abyssal Plain; (E2) a northward retroflexion along the eastern side of the Kerguelen Plateau; (E3) a leakage through gaps in the Southeast Indian Ridge, in the Australian-Antarctic Basin; (E4) a northward extension along 160°E; (P1) a northward extension toward the New Zealand; and (P2) a northeastward route from the Ross Sea along the Pacific-Antarctic

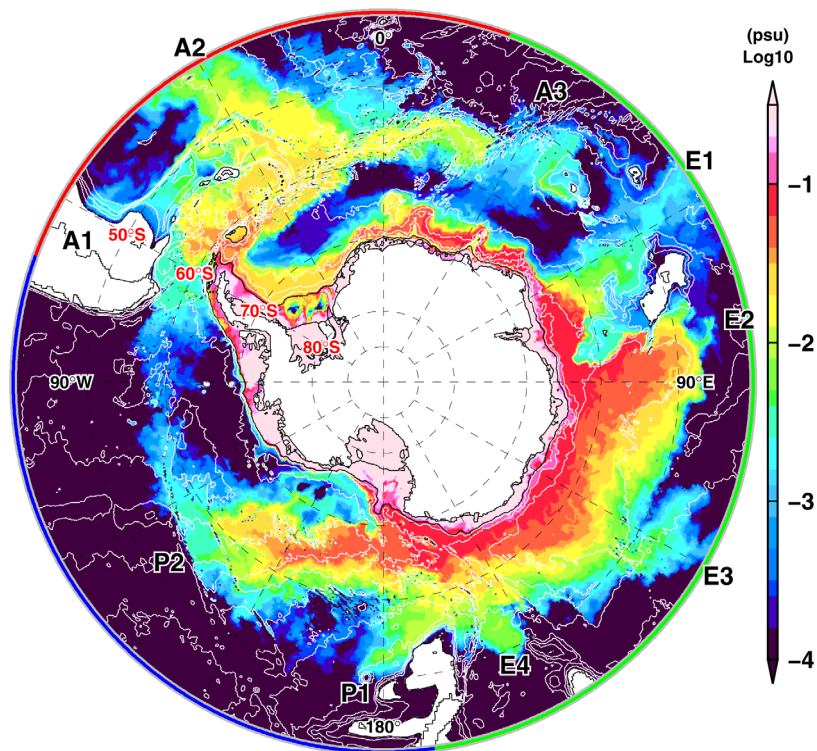


Figure 7. Horizontal distribution of the total tracer at the ocean floor at the end of a 25 year integration. The white lines show depth contours, with a 1000 m interval. The labels A1, A2, A3, E1, E2, E3, E4, P1, and P2 indicate the main pathways over the Southern Ocean. Red, green, and blue lines on the fringe indicate the Atlantic, Indian, and Pacific oceans, respectively.

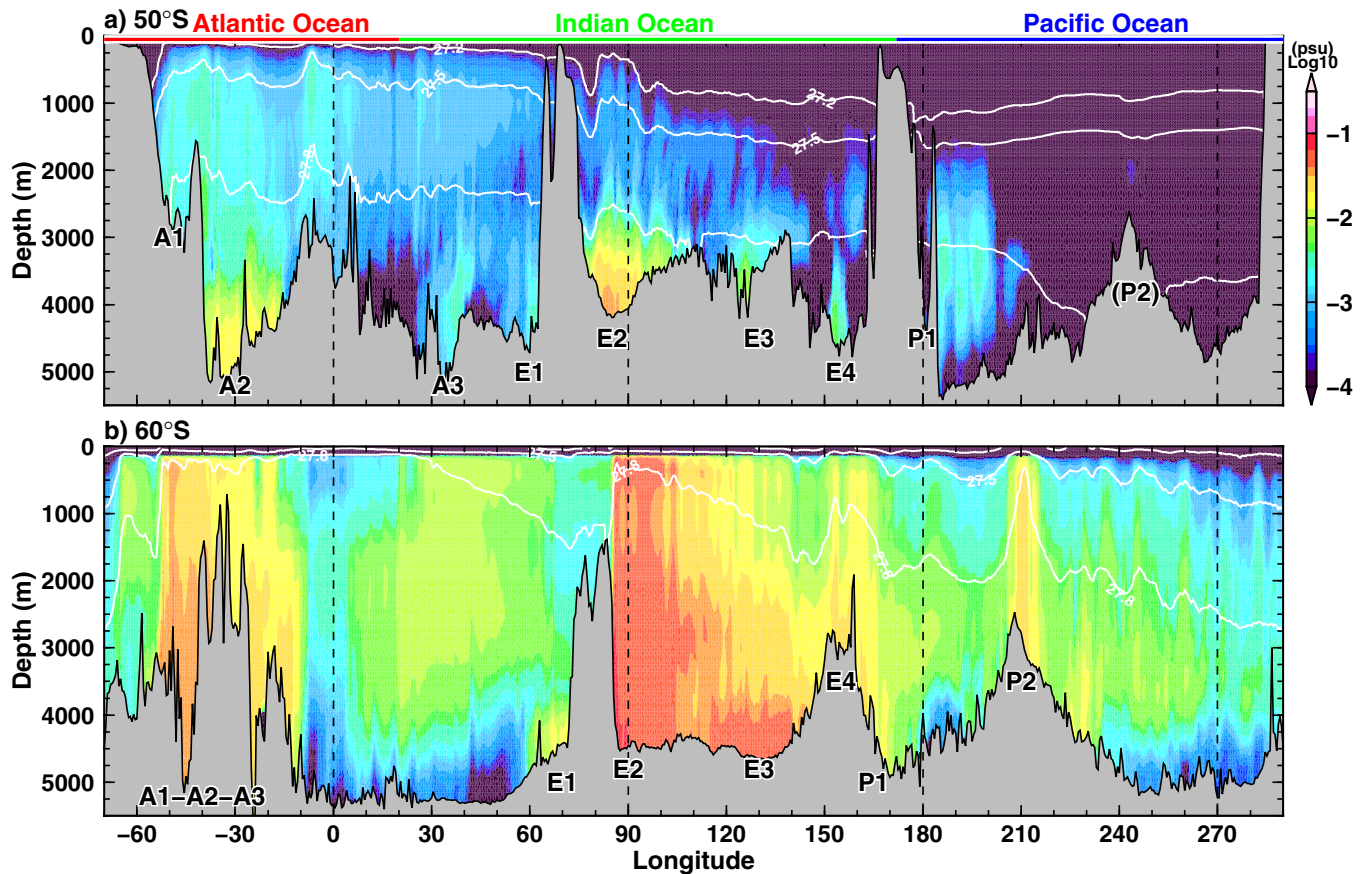


Figure 8. Vertical section of the total tracer along (a) 50°S and (b) 60°S. White contours are annual mean potential density averaged over the last 10 years (31–40 model year). The labels A1, A2, A3, E1, E2, E3, E4, P1, and P2 corresponds to those in Figure 5.

Ridge in the southeastern Pacific Basin. The model successfully reproduces the detailed spreading of DSW from Antarctic coastal margins to the deep oceans, with the distribution being consistent with the observed AABW flow patterns inferred from the distribution of CFCs [Orsi *et al.*, 1999]. These results in sections 3 and 4 provide confidence in the modeled DSW formation and spreading processes, allowing for further investigation of the regional pathways.

Vertical distributions of the total tracer along 50°S, 60°S and the shelf break are shown in Figures 8 and 9, respectively, to investigate the vertical structure of the northward extensions from the Antarctic coastal regions along the main pathways. The 1000 m contour around the Antarctic continent is used as the boundary between the Antarctic continental shelf and open ocean (i.e., as the shelf break). Along 50°S (Figure 8a),

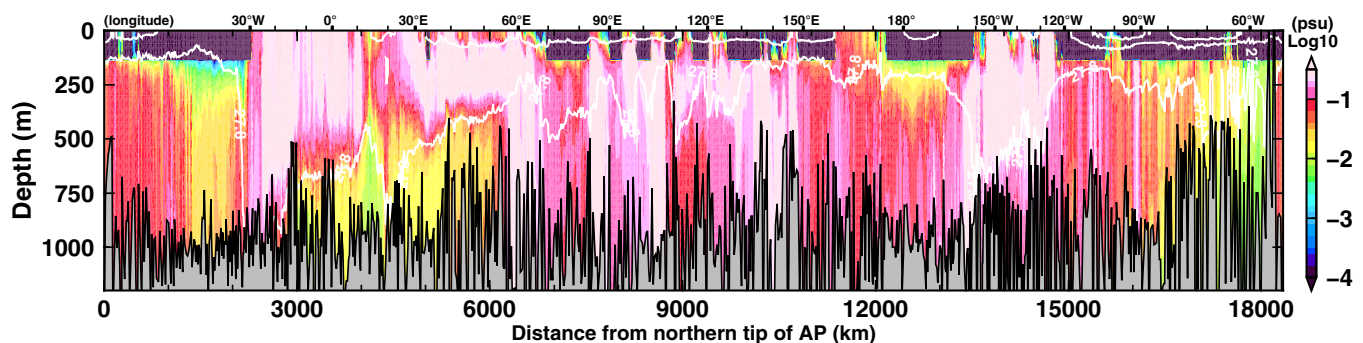


Figure 9. Vertical section of the total tracer along the 1000 m contour which encloses the Antarctic continent. White contours show the potential density surfaces of 27.20, 27.50, and 27.80 kg m^{-3} . The bottom horizontal axis indicates distance from the northern tip of the Antarctic Peninsula. The corresponding longitudes are shown in the upper axis.

high concentrations of eight pathways (A1, A2, A3, E1, E2, E3, E4, and P1) are found in bottom layers denser than the potential density 27.80 kg m^{-3} . These are strongly constrained by bottom topography (gaps or slopes). The eastward extension of the total tracer from the Ross Sea to the Pacific Ocean (P2) does not reach this latitude. A small amount of the tracer is identified in the Weddell Sea in the potential density range between 27.2 and 27.80 kg m^{-3} , reflecting the portion of the coastal tracer entrained in the Antarctic Circumpolar Current. Along 60°S (Figure 8b), trunks of these DSW pathways are identified with greater vertical extent and higher concentration. Looking at the eastern sides of several large basins (e.g., EAP, SwPB, and SePB), near-zero concentration zones ($<10^{-4}$, dark blue) are present near the ocean floor. These regions correspond to the southward flow of large-scale/regional-scale ocean gyres, which transport zero concentration water (at the initial condition) from the north.

The vertical profile of the total tracer along the shelf break (Figure 9) gives us information about DSW export regions from the Antarctic continental shelf (see also supporting information Movie). Consistent with areas of the modeled high sea ice production (Figure 1b) and the deep mixed layer depth over the continental shelf (Figure 2), high concentration zones ($>10^{-1}$, pink) are confirmed in the Weddell Sea, several parts of East Antarctica, and the Ross Sea. There are relatively low concentration zones ($\sim 10^{-2}$, green) near the ocean floor in some places (10°W – 60°E and 90°W – 60°W). These correspond to regions where southward flow of the large-scale gyre occurs. Note that since the defined position of the shelf break is located either inside or outside the tracer source regions, the surface tracer outside the source regions shows zero concentration.

4.2. Contributions of the Regional DSW to the Total Tracer

We have shown the nine routes of the total tracer over the Southern Ocean (Figure 7). Here we examine the contribution of each coastal dense shelf water source to the total tracer along the main pathways at the end of the integration (Figure 10). The time evolution of the ratio of each regional tracer, relative to the total, converges to some extent after 15 years integration. As an example, the time evolution of the ratio of tracer h is shown in Figure 11.

4.2.1. The Atlantic Ocean Routes (A1, A2, and A3)

The passive tracers released from the coastal regions a–c (Figure 1a) contribute to the bottom distribution of the total tracer along the two pathways to the Atlantic Ocean (A1 and A2) and the eastward extension along the America–Antarctica Ridge (A3) (Figures 10a–10c). The regional tracer a (east of the Antarctic Peninsula) accounts for 20–40% of the total tracer in the Argentine Basin, while the regional tracer b (in front of the Filchner–Ronne Ice Shelf) accounts for approximately 60% there. The regional tracer c (Eastern Weddell Sea) does not spread to the bottom layer near the formation region due to the low local sea ice production (Figure 1b), but the tracer dominates the bottom tracer in remote locations, i.e., under the Filchner–Ronne Ice Shelf, and in the continental shelf regions on the western side of the Weddell Sea, and the southern part of the eastward extension of A3. This indicates that dense water formation together with weak sea ice production in region c preconditions the southern and western parts of the Weddell Sea.

4.2.2. The Four Pathways to the Indian Ocean (E1, E2, E3, and E4)

The regional tracer d (from the Cape Darnley Polynya) spreads westward over the continental shelf and slope regions in the Eastern Weddell Sea, showing a dominant contribution ($\sim 80\%$) over the southern part of the Weddell Sea. A part of the tracer winds northward at about 60°E toward the Crozet Basin (E1). About 55% of the tracer from region d effectively penetrates to the deep ocean (Table 1). The distribution of the regional tracer e (Prydz Bay) is similar to that of the tracer d , but the contribution is small ($\sim 20\%$). Regional tracer f (80 – 130°E East Antarctic region) accounts for 40–50% of the total tracer on the western side of the Kerguelen Plateau and 20–30% in the coastal region of the Enderby Abyssal Plain. The low contribution of tracer e compared to tracers d and f indicates larger contributions of the coastal polynyas in the Cape Darnley region and 80 – 130°E East Antarctic regions to the bottom layer water than in the Prydz Bay regions.

The total tracer on the eastern flank of the Kerguelen Plateau (E2) is roughly explained by the two tracers g (Wilkes Land, $\sim 60\%$) and h (Ross Sea, 20–40%). The bottom total tracer over the Australian–Antarctic Basin is also dominated by these two regional tracers. Although regional tracer h contributes 20–60% off the Wilkes Land coast, most of the region in the Australian–Antarctic Basin is dominated by regional tracer g . This tracer accounts for 60–80% of the total tracer in the leakage from the gap in the southeastern Indian Ridge (E3).

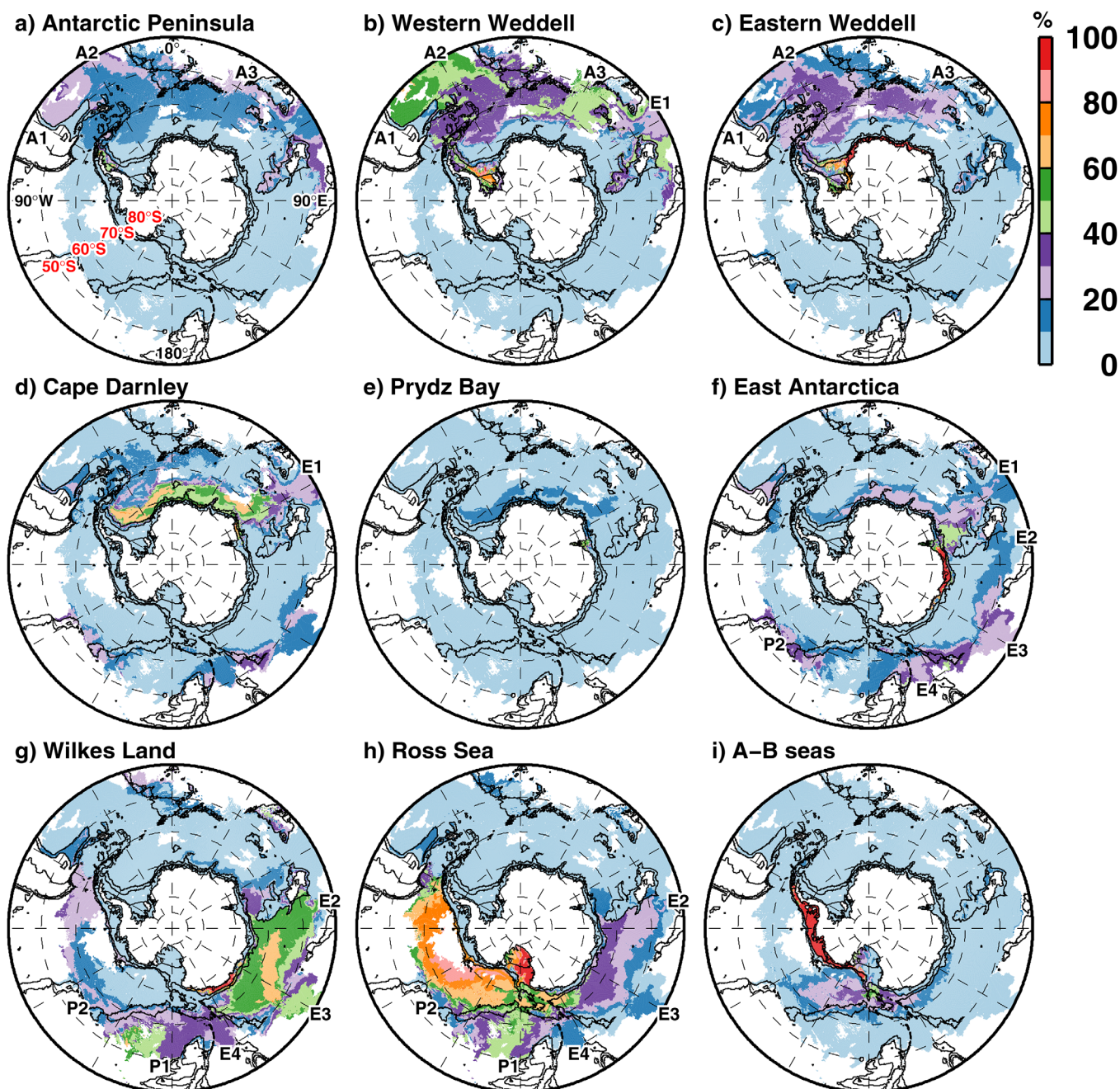


Figure 10. Maps of regional tracer at the ocean floor (percentage relative to the total tracer). Figures 10a–10i correspond to the coastal regions where each passive tracer was released (Figure 1a). Areas of the total tracer smaller than 10^{-6} are masked out. The black lines depict the 1000 and 3000 m depth contours.

Looking at the contribution on E4, tracers *g* and *h* account for 30–40% and 20% of the concentration, respectively. Almost half of the total tracer on the route is explained by the remote sources of tracers *d* and *f*. A part of the remote tracers is transported by the eastward flowing Antarctic Circumpolar Current at intermediate depths and contribute to this route in an indirect way.

4.2.3. The Two Routes to the Pacific Ocean (P1 and P2)

Regional tracers *g* and *h* play a major role in the two routes to the Pacific Ocean. Since there is strong sea ice formation in front of the Ross Ice Shelf, tracer *h* is effectively transported to the bottom layer (Table 1) and largely contributes to the two branches toward the Pacific Ocean. Regional tracer *g* contributes to the northern parts of the branches through a deeper part of the Antarctic Circumpolar Current. Regional tracer *i*

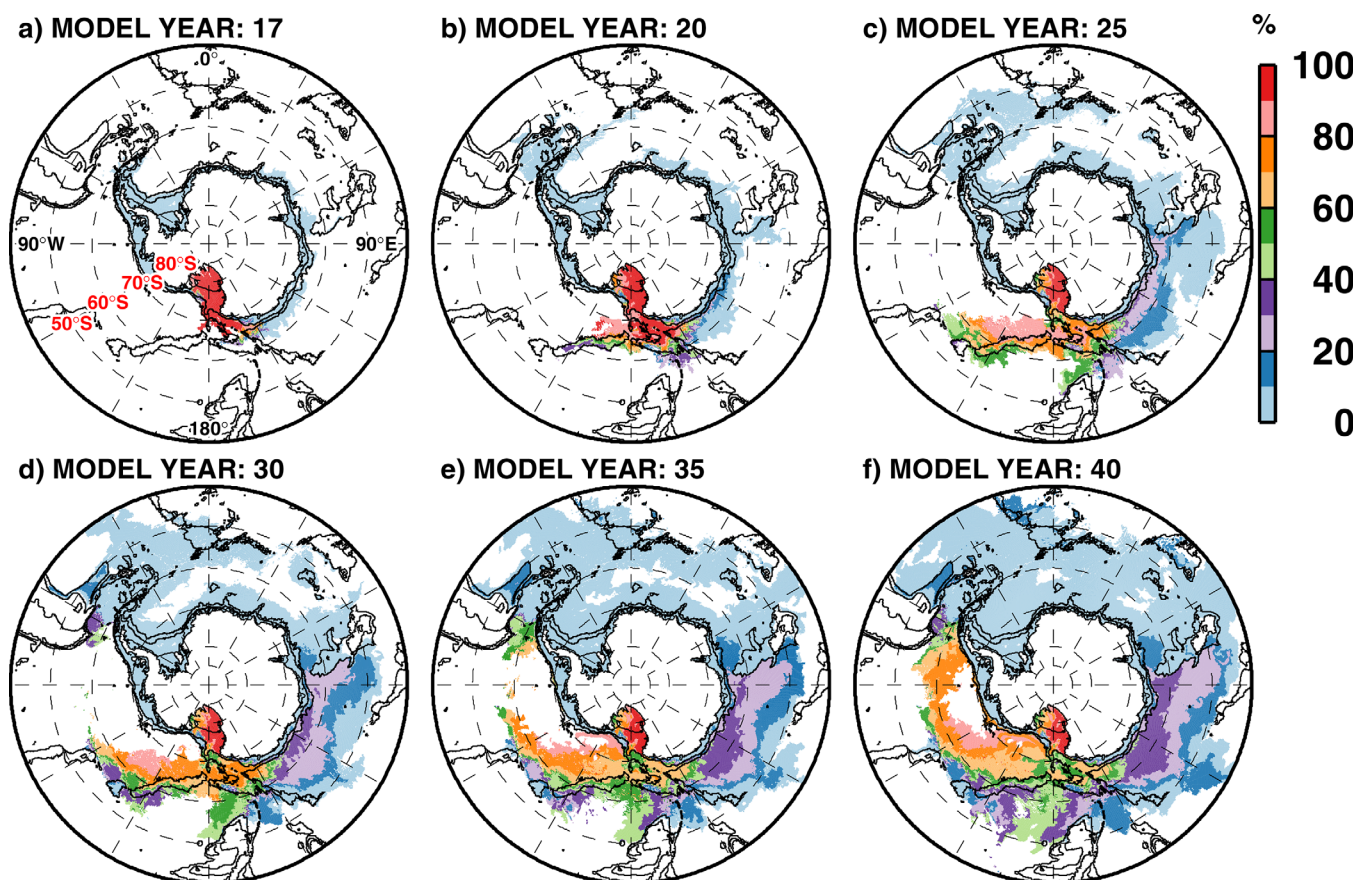


Figure 11. Snapshots of the ratio of the regional tracer h at the ocean floor (17, 20, 25, 30, 35, and 40 model year). Areas of the total tracer at the ocean floor smaller than 10^{-6} are masked out. The black lines depict the 1000 and 3000 m depth contours.

(Amundsen-Bellinghousen seas) is confined to the continental shelf region, but a part of the tracer is advected westward to the Ross Sea over the continental shelf region and partly contributes to the total tracer in the southern and western parts of the Ross Sea.

5. Summary and Discussion

We have conducted a detailed investigation of the pathways of DSW on the decadal timescale over the Southern Ocean, based on passive tracer experiments of dense shelf waters released over Antarctic continental shelf regions in a coupled ocean-sea ice-ice shelf model (see Figure 1a for the defined coastal regions). The total tracer is effectively transported into the bottom layer through deep convection over the continental shelf regions (Figure 2), across the shelf break (Figure 9), and spreads northward (Figures 4, 5, and 8) with deep thermohaline circulation (Figure 3). The bottom distribution of the total tracer (Figure 7) is similar to the observed distribution of AABW, inferred from the distribution of CFCs [Orsi *et al.*, 1999]. The model shows nine main pathways of the passive tracer over the Southern Ocean along the bottom topography: three routes toward to the Atlantic Ocean, four routes toward to the Indian Ocean, and two routes toward to the Pacific Ocean. The comprehensive tracer experiments enable a quantitative examination of the detailed pathways of DSW spreading from local source regions to the deep ocean (Figure 10). The model demonstrates that the distribution of DSW to deep layers strongly depends on the coastal formation regions (Table 1). These results suggest that local changes in sea ice production and DSW formation on the continental shelf propagate to the deep ocean along the particular pathway of the regional DSW.

While we could examine the detailed pathways of DSW from Antarctic coastal polynya based on passive tracer experiments, our focus in this study is limited to the decadal timescale (Figures 6 and 11 and supporting information Movie) rather than a steady state or centennial timescale, due to our use of a regional Southern Ocean

model. An integration over hundreds to a thousand years with a high-resolution global ocean-sea ice model is required to fully analyze spreading of Antarctic dense waters to the world ocean abyss.

A study of AABW pathways by *Van Sebille et al.* [2013] showed a spatial map of probability of Lagrangian parcels in AABW layers and concluded that approximately 70% of AABW experiences at least one loop in the Antarctic Circumpolar Current regions before reaching subtropical basins. Our DSW distribution (Figure 7) is somewhat different from their AABW distribution (see Figure 2 in *Van Sebille et al.* [2013]) because the targeted water masses are disparate in the two studies. In this study, we traced water masses transformed by high salinity input in coastal polynyas over the Antarctic continental shelf, while they traced water masses modified over continental shelf, slope, and rise (i.e., including mixing processes of DSW, AASW, and CDW south of 60°S) to assess all water masses contributing AABW to lower latitudes. The main difference in the two studies suggests that our results correspond to the denser part of AABW which is transported directly to the subtropical basins (30% of AABW estimated in *Van Sebille et al.* [2013]), being strongly constrained by bottom topography.

There are some limitations to the model configuration used in this study. Although our model does reproduce high sea ice production and DSW formation in Antarctic coastal polynyas with a horizontal resolution limited to 10–20 km near the Antarctic coast, the resolution is not sufficient to resolve ocean eddies and small-scale bottom topography (a few kilometers). These unresolved processes and topography could further modify water-mass exchange across the shelf break and the offshore transport of the oceanic tracers [*St-Laurent et al.*, 2013; *Stewart and Thompson*, 2015]. A similar limitation is also present in the vertical resolution. We have a z-coordinate system in the ocean model, where high vertical resolution is necessary to represent the downslope flow of dense water [*Wang et al.*, 2008]. While we used a relatively high vertical resolution of 40 m over the upper continental slope regions, this is insufficient and leads to excessive dilution of coastal DSW through mixing with different water masses over the continental slope and rise regions. In fact, our modeled deep meridional circulation decreases in magnitude from 10 Sv at 60°S to only a few Sv at 55°S (Figure 3). This pronounced reduction may be caused by the model's resolution.

Furthermore, our tracer experiments also have limitations. Although our modeled DSW pathways have shown similarities with the observed AABW flow patterns, in reality, several other water masses (e.g., CDW, ice shelf

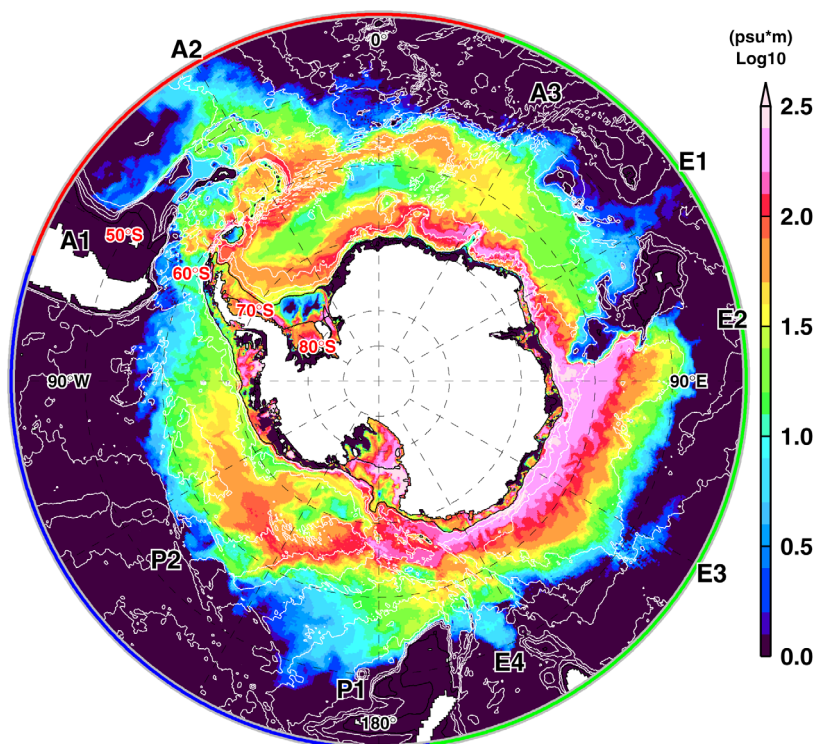


Figure A1. Horizontal distribution of the total tracer integrated in the layer denser than 27.80 kg m^{-3} .

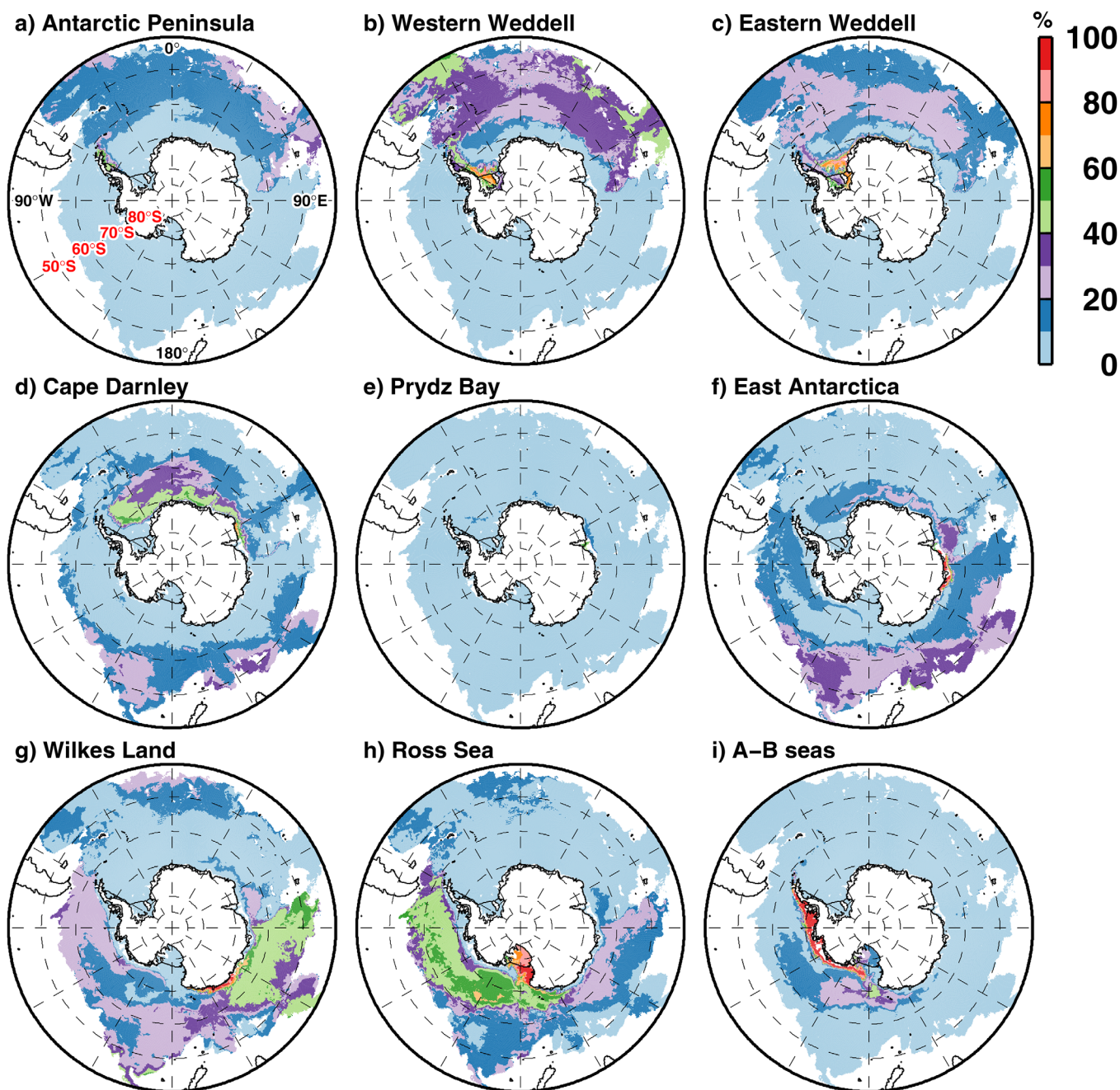


Figure A2. Same as Figure 10, but for the tracer integrated in the layer denser than 27.80 kg m^{-3} .

water, and intermittent dense water formed in open water convection) also play important roles in AABW formation processes. Therefore, our coastal DSW tracer experiments, combined with the limitation of the decadal integration in a regional Southern Ocean model, cannot be used for a full assessment of AABW production.

Sea ice production along Antarctic coastal margins is a key critical parameter for dense water formation and basal melting at ice shelves, both of which contribute to the strength of ocean's thermohaline circulation. Monitoring changes in the coastal icescape [Barber and Massom, 2007] and associated sea ice production, as well as direct ocean properties, is necessary for a better understanding of Antarctic and the Southern Ocean climate. Numerical modeling with continuous development is an invaluable tool for detecting, assessing, and understanding the Southern Ocean system and its change and variability.

Appendix A: Tracer Distributions in the Layer Denser Than 27.80 kg m^{-3}

In the main text, we use the horizontal distributions at the ocean floor to describe pathways of the total and regional DSW tracers. In this appendix, we show horizontal distributions in the layer denser than 27.80 kg m^{-3} . As shown in Figure 6, more than 70% of the total tracer at the end of the integration is in this dense layer. Regarding general patterns, both the horizontal distributions of the total tracer (Figure A1) and the ratio of the regional tracers (Figure A2) are similar to those at the ocean floor (Figures 7 and 10). However, the integrated tracer distribution is more extensive than the bottom one due to the rapid transport by the eastward flowing Antarctic Circumpolar Current at intermediate depths. Therefore, the contrast of the regional ratios becomes smaller than those at the ocean floor (Figure A2).

Acknowledgments

This research was supported by the Australian Government's Cooperative Research Centre through the ACE CRC, and contributes to ACE CRC Project R1.3, AAS 4116 and WCRP CliC "targeted activity" Linkages between Cryosphere Elements. K.K. and T.T. were supported by the Canon Foundation. G.W. was supported by the Australian Research Council's Future Fellowship program. H.H. was supported by JSPS KAKENHI grant 26247980. Special thanks to Simon Marsland for providing constructive comments on an earlier version of the manuscript. The RTopo1 data were acquired from: <https://doi.pangaea.de/10.1594/PANGAEA.741917> and the PHC data from: http://psc.apl.washington.edu/nonwp_projects/PHC/Climatology.html. The climatological surface boundary forcing data were obtained from <http://www.omip.zmaw.de/>. The sea ice concentration data set, derived using with the NASA Team algorithm, was obtained from ftp://sidads.colorado.edu/pub/DATASETS/nsidc0051_gsfc_nasateam_seaice.

References

- Aoki, S., S. R. Rintoul, S. Ushio, S. Watanabe, and N. L. Bindoff (2005), Freshening of the Adélie Land Bottom Water near 140°E , *Geophys. Res. Lett.*, *32*, L23601, doi:10.1029/2005GL024246.
- Baines, P. G., and S. Condie (1998), Observations and modelling of Antarctic downslope flows: A review, in *Ocean, Ice and Atmosphere: Interactions at the Antarctic Continental Margin*, vol. 75, pp. 29–49, American Geophysical Union, Washington, D. C.
- Barber, D. G., and R. A. Massom (2007), Chapter 1. The role of sea ice in Arctic and Antarctic polynyas, in *Polynyas: Windows to the World*, vol. 74, pp. 1–54, Elsevier, Amsterdam, Netherlands.
- de Boyer Montégut, C., G. Madec, A. S. Fischer, A. Lazar, and D. Iudicone (2004), Mixed layer depth over the global ocean: An examination of profile data and a profile-based climatology, *J. Geophys. Res.*, *109*, C12003, doi:10.1029/2004JC002378.
- Doney, S. C., and M. W. Hecht (2002), Antarctic bottom water formation and deep-water chlorofluorocarbon distributions in a global ocean climate model, *J. Phys. Oceanogr.*, *32*, 1642–1666.
- Jacobs, S. S. (2004), Bottom water production and its links with the thermohaline circulation, *Antarct. Sci.*, *16*(4), 427–437, doi:10.1017/S095410200400224X.
- Jacobs, S. S., H. H. Hellmer, C. S. M. Doake, A. Jenkins, and R. M. Frolich (1992), Melting of ice shelves and the mass balance of Antarctica, *J. Glaciol.*, *38*(130), 375–387, doi:10.1038/228047a0.
- Johnson, G. C. (2008), Quantifying Antarctic Bottom Water and North Atlantic Deep Water volumes, *J. Geophys. Res.*, *113*, C05027, doi:10.1029/2007JC004477.
- Kusahara, K., and H. Hasumi (2013), Modeling Antarctic ice shelf responses to future climate changes and impacts on the ocean, *J. Geophys. Res. Oceans*, *118*, 2454–2475, doi:10.1002/jgrc.20166.
- Kusahara, K., and H. Hasumi (2014), Pathways of basal meltwater from Antarctic ice shelves: A model study, *J. Geophys. Res. Oceans*, *119*, 5690–5704, doi:10.1002/2014JC009915.
- Kusahara, K., H. Hasumi, and T. Tamura (2010), Modeling sea ice production and dense shelf water formation in coastal polynyas around East Antarctica, *J. Geophys. Res.*, *115*, C10006, doi:10.1029/2010JC006133.
- Kusahara, K., H. Hasumi, and G. D. Williams (2011), Dense shelf water formation and brine-driven circulation in the Adélie and George V Land region, *Ocean Model.*, *37*(3–4), 122–138, doi:10.1016/j.ocemod.2011.01.008.
- Kusahara, K., T. Sato, A. Oka, T. Obase, R. Greve, A. Abe-Ouchi, and H. Hasumi (2015), Modelling the Antarctic marine cryosphere at the Last Glacial Maximum, *Ann. Glaciol.*, *56*(69), 425–435, doi:10.3189/2015AoG69A792.
- Marsland, S. J., N. L. Bindoff, G. D. Williams, and W. F. Budd (2004), Modeling water mass formation in the Mertz Glacier Polynya and Adélie Depression, East Antarctica, *J. Geophys. Res.*, *109*, C11003, doi:10.1029/2004JC002441.
- Marsland, S. J., J. A. Church, N. L. Bindoff, and G. D. Williams (2007), Antarctic coastal polynya response to climate change, *J. Geophys. Res.*, *112*, C07009, doi:10.1029/2005JC003291.
- Massom, R. A., P. T. Harris, K. J. Michael, and M. J. Potter (1998), The distribution and formative processes of latent-heat polynyas in East Antarctica, *Ann. Glaciol.*, *27*, 420–426.
- Morales Maqueda, M. A., A. J. Willmott, and N. R. T. Biggs (2004), Polynya dynamics: A review of observations and modeling, *Rev. Geophys.*, *42*, RG1004, doi:10.1029/2002RG000116.
- Nihashi, S., and K. I. Ohshima (2015), Circumpolar mapping of Antarctic coastal polynyas and landfast sea ice: Relationship and variability, *J. Clim.*, *28*(9), 3650–3670, doi:10.1175/JCLI-D-14-00369.1.
- Noh, Y., and H. J. Kim (1999), Simulations of temperature and turbulence structure of the oceanic boundary layer with the improved near-surface process, *J. Geophys. Res.*, *104*, 15,621.
- Orsi, A. H., G. C. Johnson, and J. L. Bullister (1999), Circulation, mixing, and production of Antarctic Bottom Water, *Prog. Oceanogr.*, *43*(1), 55–109, doi:10.1016/S0079-6611(99)00004-X.
- Orsi, A. H., W. M. Smethie, and J. L. Bullister (2002), On the total input of Antarctic waters to the deep ocean: A preliminary estimate from chlorofluorocarbon measurements, *J. Geophys. Res.*, *107*(C8), doi:10.1029/2001JC000976.
- Purkey, S. G., and G. C. Johnson (2013), Antarctic bottom water warming and freshening: Contributions to sea level rise, ocean freshwater budgets, and global heat gain, *J. Clim.*, *26*(16), 6105–6122, doi:10.1175/JCLI-D-12-00834.1.
- Rintoul, S. R. (2007), Rapid freshening of Antarctic Bottom Water formed in the Indian and Pacific oceans, *Geophys. Res. Lett.*, *34*, L06606, doi:10.1029/2006GL028550.
- Röske, F. (2006), A global heat and freshwater forcing dataset for ocean models, *Ocean Model.*, *11*(3–4), 235–297, doi:10.1016/j.ocemod.2004.12.005.
- Santoso, A., and M. H. England (2008), Antarctic Bottom Water variability in a coupled climate model, *J. Phys. Oceanogr.*, *38*(9), 1870–1893, doi:10.1175/2008JPO3741.1.
- Sasai, Y., A. Ishida, Y. Yamanak, and H. Sasaki (2004), Chlorofluorocarbons in a global ocean eddy-resolving OGCM: Pathway and formation of Antarctic Bottom Water, *Geophys. Res. Lett.*, *31*, L12305, doi:10.1029/2004GL019895.
- Schmitz, W. J. (1995), On the interbasin-scale thermohaline circulation, *Rev. Geophys.*, *33*(2), 151–173, doi:10.1029/95RG00879.
- Sigman, D. M., and E. A. Boyle (2000), Glacial/interglacial variations in atmospheric carbon dioxide, *Nature*, *407*(6806), 859–869, doi:10.1038/35038000.

- St-Laurent, P., J. M. Klinck, and M. S. Dinniman (2013), On the role of coastal troughs in the circulation of warm Circumpolar Deep Water on Antarctic shelves, *J. Phys. Oceanogr.*, *43*(1), 51–64, doi:10.1175/JPO-D-11-0237.1.
- Steele, M., M. Steele, R. Morley, R. Morley, W. Ermold, and W. Ermold (2001), b. PHC: A global ocean hydrography with a high quality Arctic Ocean, *J. Clim.*, *14*, 2079–2087, doi:10.1175/1520-0442.
- Stewart, A. L., and A. F. Thompson (2015), Eddy-mediated transport of warm Circumpolar Deep Water across the Antarctic Shelf Break, *Geophys. Res. Lett.*, *42*, 432–440, doi:10.1002/2014GL062281.
- Tamura, T., K. I. Ohshima, and S. Nihashi (2008), Mapping of sea ice production for Antarctic coastal polynyas, *Geophys. Res. Lett.*, *35*, L07606, doi:10.1029/2007GL032903.
- Timmermann, R., et al. (2010), A consistent dataset of Antarctic ice sheet topography, cavity geometry, and global bathymetry, *Earth Syst. Sci. Data Discuss.*, *3*(2), 231–257, doi:10.5194/essdd-3-231-2010.
- Van Sebille, E., P. Spence, M. R. Mazloff, M. H. England, S. R. Rintoul, and O. A. Saenko (2013), Abyssal connections of Antarctic bottom water in a Southern Ocean State Estimate, *Geophys. Res. Lett.*, *40*, 2177–2182, doi:10.1002/grl.50483.
- Violaine, P., S. Jean-Baptiste, S. Sunke, R. Fabien, and J. B. Charrassin (2017), The ocean mixed layer under Southern Ocean sea-ice: Seasonal cycle and forcing, *J. Geophys. Res. Oceans*, *122*, 1608–1633, doi:10.1002/2016JC011970.
- Wang, Q., S. Danilov, and J. Schröter (2008), Comparison of overflow simulations on different vertical grids using the Finite Element Ocean circulation Model, *Ocean Model.*, *20*(4), 313–335, doi:10.1016/j.ocemod.2007.10.005.